Electronic Supplementary Material (ESI) for ChemComm.

Supporting Information

Revealing the Crystal Phases of Primary Particles Formed during the Coprecipitation of Iron Oxides

Yu Mao, Zuoheng Zhang, Hongfeng Zhan, Jianfei Sun, Yan Li, Zhenhuang Su, Yonghua Chen, Xingyu Gao, Xiao Huang* and Ning Gu*

Experimental Section

Chemicals: Ferric chloride hexahydrate (99.95 %, $FeCl_3 \bullet 6H_2O$) was purchased from Acros Organics, ferrous chloride tetrahydrate (99+ %, $FeCl_2 \bullet 4H_2O$) was purchased from Macklin, Hydrochloric acid (36 %-38 %, HCl) was purchased from Sinopharm Chemical Reagent Co.,Ltd, and polyglucose sorbitol carboxymethyether (PSC, Mw ~ 10000, the coating materials of Ferumoxytol) was supplied by Chiatai Tianqing Pharmaceutical Group Co., Ltd. All reagents were used as received without further purification. Ultrapure water was used throughout the experiments. The NH_3 and N_2 gases were high purity.

Gas/Liquid Mixed Phase Fluidic Reactor: Some microfluidic devices including single-phase fluidic systems and droplet-based fluidic systems have been used to synthesize iron oxide nanoparticles via coprecipitation method by using some alkaline solution[1-3]. However, the single-phase fluidic systems are usually subjected to diffusion-limited mixing, and conventional oil/water droplet-based fluidic systems facing the problem of product separation. Thus, the alkaline gas NH_3 was chosen as a gas phase reactant to construct a gas/liquid mixed phase fluidic reactor which could avoid the forementioned problems. The gas/liquid mixed phase fluidic reactor was constructed with a typical T-shaped channel which was made of polytetrafluoroethylene (PTFE) and with 2.5 mm of inner diameter (ID). Reaction gas and iron precursor solution were pumped into the T-shaped channel through inlet 1 and inlet 2 respectively via PTFE tubes as Figure 1 shows. The reaction gas was composed of NH_3 and N_2, their fluxes were controlled via gas mass flow meters (Beijing Sevenstar Flow Co., Ltd.). The flow rate of iron precursor solution was controlled via a precision piston pump (Corning UI-22). The PTFE tube (ID = 2.2 mm) was connected to the outlet of T-shaped channel and leaded to a sample flask.

Control Synthesis of the Primary IONPs: The iron precursor solutions contain Fe^{3+} (0.02 / 0.20 mM) and Fe^{2+} (0.01 / 0.10 mM) were prepared by ultrasonic dissolving a certain weight of $FeCl_3 \bullet 6H_2O$ and $FeCl_2 \bullet 4H_2O$ in ultrapure water. A certain weight of PSC were firstly dissolved in ultrapure water and then mixed with the iron precursor solutions, the weight ratio of PSC / $FeCl_3 \bullet 6H_2O$ was set as 4 / 3 according to our previous researches. All reaction solutions were deoxygenated via N_2 bubbling for at least 30 min before reaction. The flux of NH_3 was set as 11 sccm, the flux of N_2 was set as 7 sccm, the flow rate of iron precursor solutions was set as 2 mL/min, the corresponding residence time of reaction solutions in 15 cm, 4 m, 10 m, 15 m and 20 m PTFE tubes were about 3 s, 1 min, 2 min 30 s, 4 min 12 s and 5 min 40 s respectively. The products were collected in a sample flask which was immersed in - 10 ℃ alcohol bath to quench the reactions. The pH of droplets flowed out the reactor were randomly tested using pH test strips as Figure

S1 shows. The as-prepared products were were repeatedly washed with ultrapure water and concentrated by centrifugal ultrafiltration (Millipore, molecular size cutoff of 30 kDa) for many times to get rid of excess ions. The centrifuge was proceeded at 0 ℃ with rotational speed of 5000 rpm for 6 min every time.

Characterization Methods: The morphology and size distribution of primary IONPs were determined by a FEI TEM (Talos F200X) operated at 200 kV. At least 100 of IONPs were measured to evaluate the mean diameter and particle size distribution. The HRTEM was performed to determine the crystal structure of primary IONPs using a spherical aberration corrected transmission electron microscope (Titan 80-300) operated at 300 kV. VESTA[4] was used for preparation of the schematic lattice models. The lyophilized dry powders of samples were prepared by using a lyophilizer (Advantage 20EL-85, SP Scientific). The composition and structure of samples were also tested as lyophilized dry powders by synchrotron X-ray diffraction analysis, which performed on the X-ray diffraction beamline of BL14B1 at Shanghai Synchrotron Radiation facility (SSRF), the test energy is 10 keV, the X-ray wavelength is 1.24 Å and transformed to have a 2-Theta from the wavelength of Cu Kα (1.54 Å). The UV-vis spectra were measured by a UV–vis spectrophotometer (UV-3600, Shimadzu). The pH was tested by a pH meter (FE20, METTLER TOLEDO).

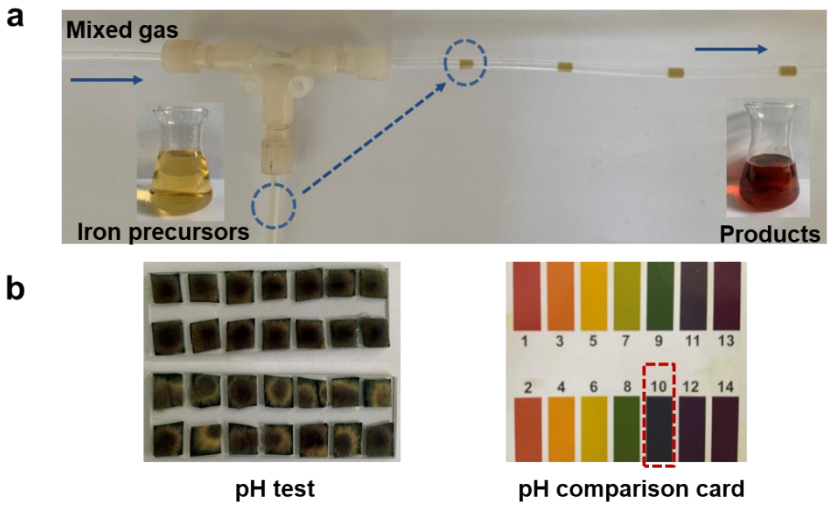

Fig.S1 (a) The gas/liquid mixed phase fluidic reactor and (b) photograph of pH tests of the droplets by using pH comparison card. After the reaction proceeded in the gas/liquid mixed phase fluidic reactor, the initial transparent light yellow precursor solution became red-brownish. The precursor solution containing 2 mM Fe^{2+}, 4 mM Fe^{3+} and 1.44 mg/mL PSC. The measured pH values of the final product and randomly chosen intermediate droplets are all about 10.

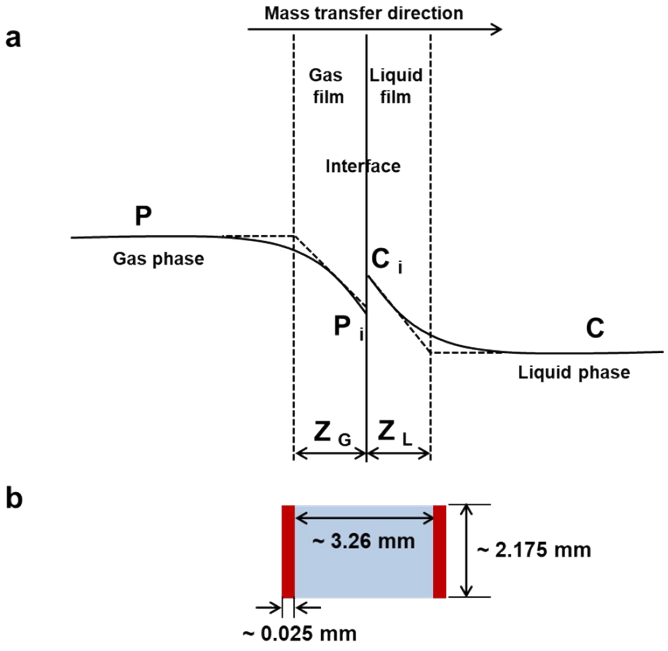

Fig.S2 (a) Schematic diagram describing the two-film theory for gas/liquid interface; (b) Schematic illustration of the diffusion layers (red) and stable region (blue) of the liquid slug.

Two-film theory[5, 6] calculation based on Figure S2:

The ionization of $NH_3 \cdot H_2O$:

$$NH_3 \cdot H_2O = NH_4^+ + OH^-$$

$$Kb = \frac{C(NH4+) \cdot C(OH-)}{C - C(NH3)}$$

Given that $K_b = 1.76 \times 10^{-5}$, when pH = 10, $C(NH_4^+) = C(OH^-) = C(NH_3) = 1.0 \times 10^{-4}$ mol / L, C is calculated to be 6.68×10^{-4} mol / L.

The thickness of the liquid diffusion layer can be calculated based on the two-film theory (Figure S2a).

$$KL = \frac{D \cdot C0}{ZL \cdot CB}$$

$$CB = \frac{\rho(H2O)}{M(H2O)}$$

$$C0 = CB + C$$

The thickness of liquid diffusion layer Z_L was calculated to be about 0.025 mm based on the reference data listed below. This value is much smaller than the length of liquid slug (~ 3.26 mm, Figure S2b). When the reaction pH is ~ 11 as Table S1 shows, the Z_L was also calculated as ~ 0.025 mm. Therefore, the concentration distribution of NH_3 in the liquid slugs can be considered homogeneous.

Reference data [5, 6]:

C (NH_3): Concentration of ionized $NH_3 \cdot H_2O$ in liquid phase (mol / L)

C (NH_4^+) : Concentration of NH_4^+ in liquid phase (mol / L)

C (OH^-) : Concentration of OH^- in liquid phase (mol / L)

C : Concentration of NH3 in liquid phase (mol / L)

K_b: The ionization constant of $NH_3 \cdot H_2O$, 1.76×10^{-5}

K_L: Liquid film mass transfer coefficient, 6.94×10^{-5} m ▪ s^{-1}

D: Diffusion coefficient of NH_3 in water, 1.76×10^{-9} m^2 ▪ s^{-1}

ρ (H_2O): The density of water, 1000 g / L

M (H_2O): The molecular weight of water, 18 g / mol

C_0: The whole concentration in diffusion layer (mol / L)

C_B: The concentration of absorbent in diffusion layer (mol / L)

Z_L: The thickness of liquid film (mm)

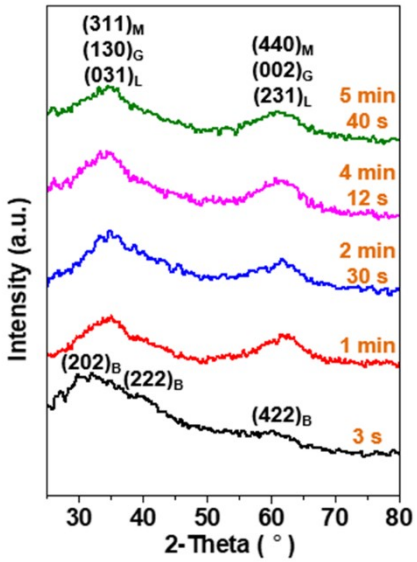

Fig.S3 Synchrotron X-ray diffraction patterns of primary IONPs prepared with 0.03 mM iron precursor at different reaction time.The subscription B, G, L and M represent the $Fe(OH)_3$ (JCPDS no. 46-1436), α-FeOOH (JCPDS no. 29-0713), γ-FeOOH (JCPDS no. 76-2301), and Fe_3O_4 (JCPDS no. 19-0629) phases, respectively.

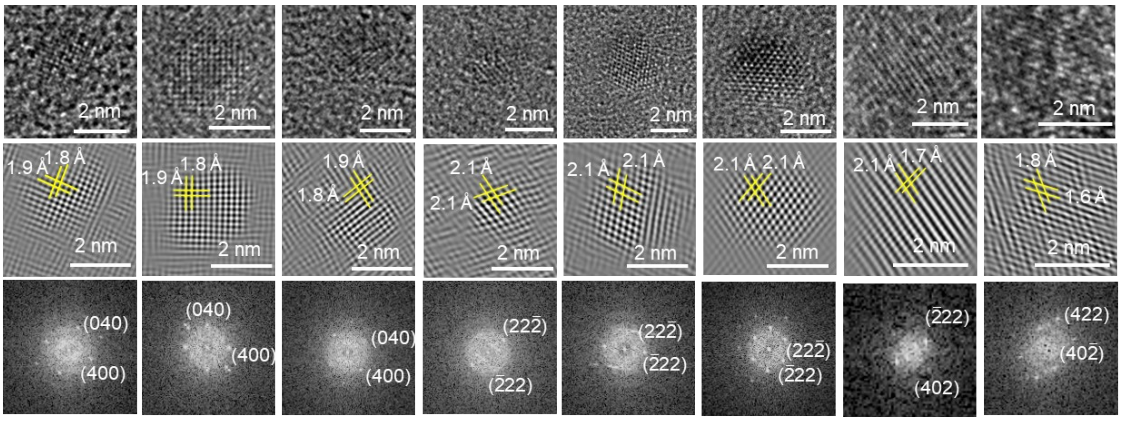

Fe(OH)$_3$ [001] Fe(OH)$_3$ [001] Fe(OH)$_3$ [001] Fe(OH)$_3$ [101] Fe(OH)$_3$ [101] Fe(OH)$_3$ [101] Fe(OH)$_3$ [$\bar{1}$3$\bar{2}$] Fe(OH)$_3$ [1$\bar{4}\bar{2}$]

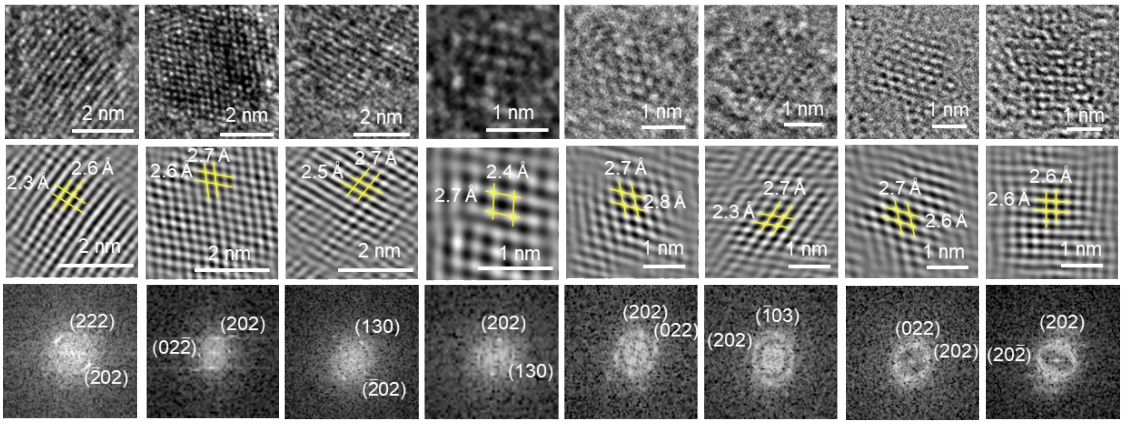

Fe(OH)$_3$ [1-21] Fe(OH)$_3$ [$\bar{1}$11] Fe(OH)$_3$ [3$\bar{1}$3] Fe(OH)$_3$ [3$\bar{1}$-3] Fe(OH)$_3$ [$\bar{1}\bar{1}$1] Fe(OH)$_3$ [0$\bar{1}$0] Fe(OH)$_3$ [$\bar{1}\bar{1}$1] Fe(OH)$_3$ [010]

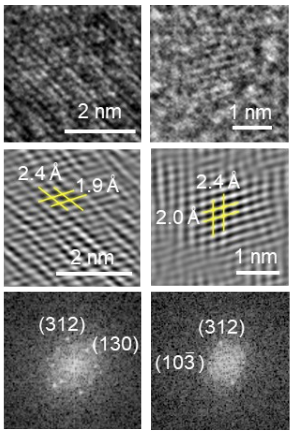

Fe(OH)$_3$ [3$\bar{1}\bar{4}$] Fe(OH)$_3$ [$\bar{3}$11$\bar{1}$]

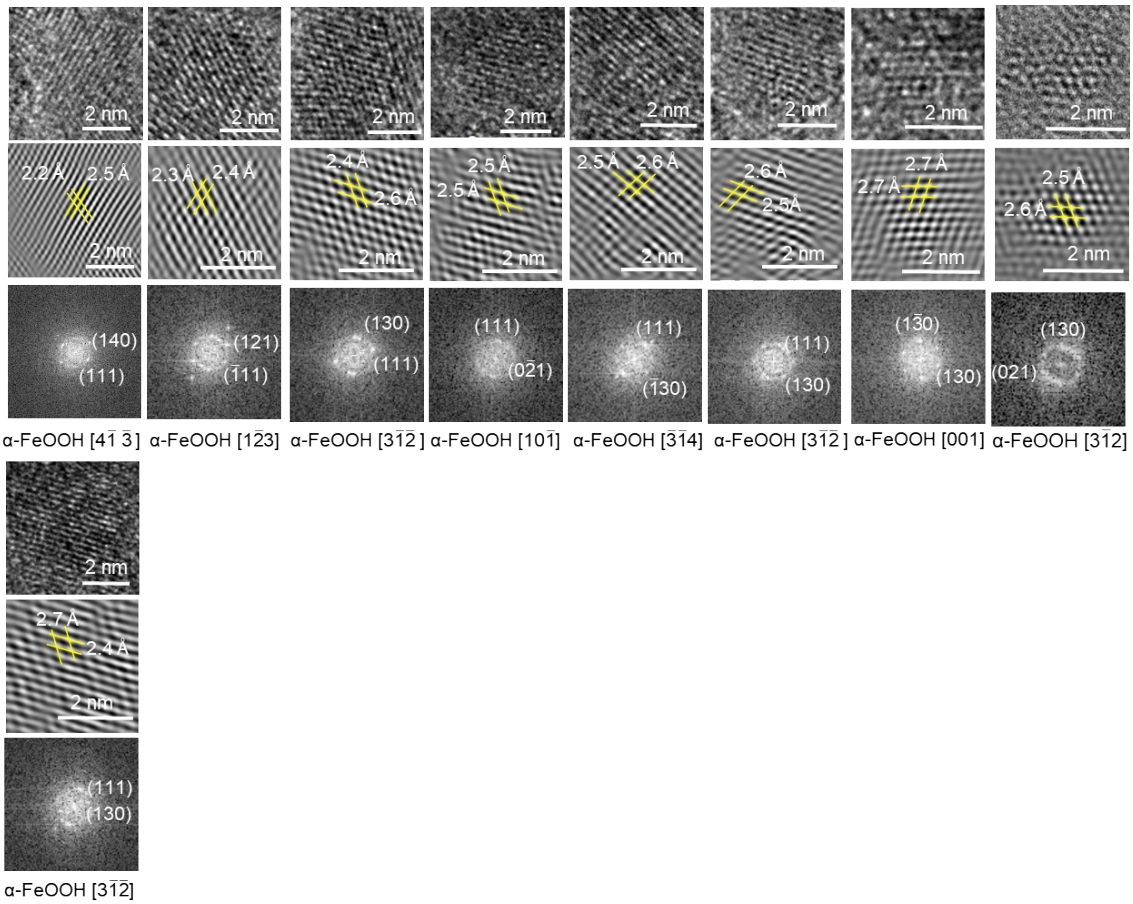

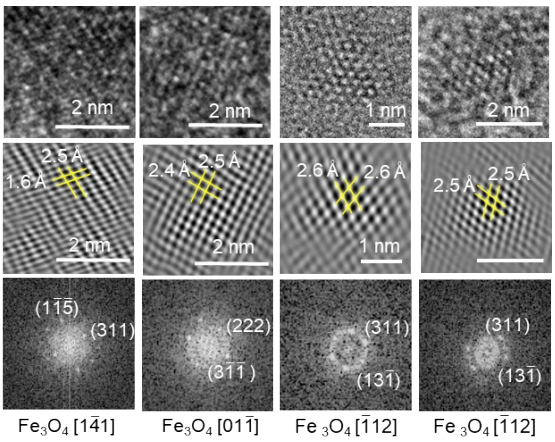

Fig.S4 High resolution SACTEM analysis of the primary IONPs prepared with 0.03 mM reaction concentration at ~ 3 s.

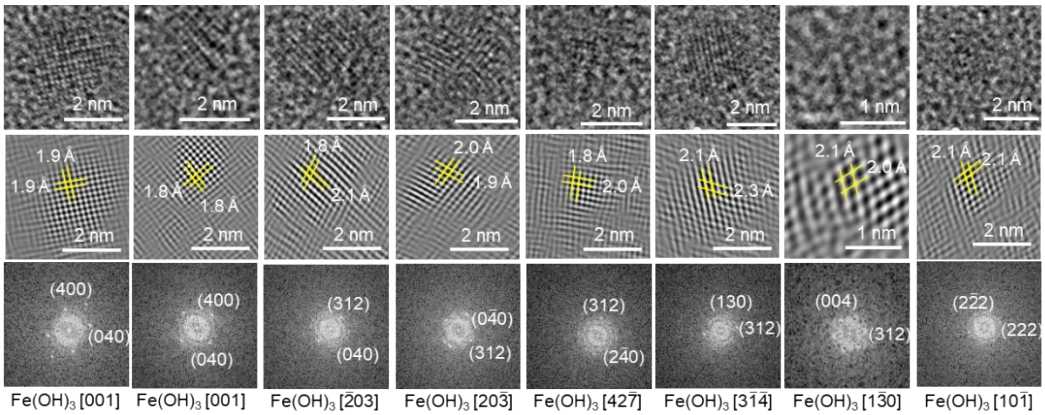
Fe(OH)3 [001]
Fe(OH)3 [001]
Fe(OH)3 [2̄03]
Fe(OH)3 [203]
Fe(OH)3 [42̄7]
Fe(OH)3 [3̄1̄4]
Fe(OH)3 [1̄30]
Fe(OH)3 [10̄1̄]

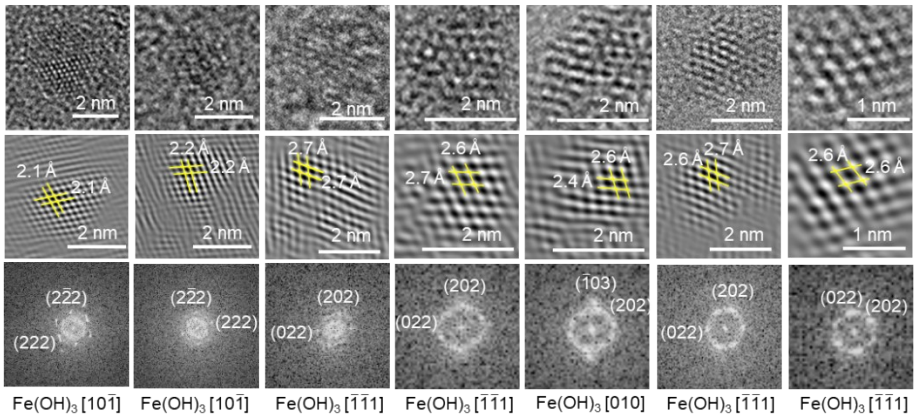
Fe(OH)3 [10̄1̄]
Fe(OH)3 [10̄1̄]
Fe(OH)3 [1̄1̄1]
Fe(OH)3 [1̄1̄1]
Fe(OH)3 [010]
Fe(OH)3 [1̄1̄1]
Fe(OH)3 [1̄1̄1]

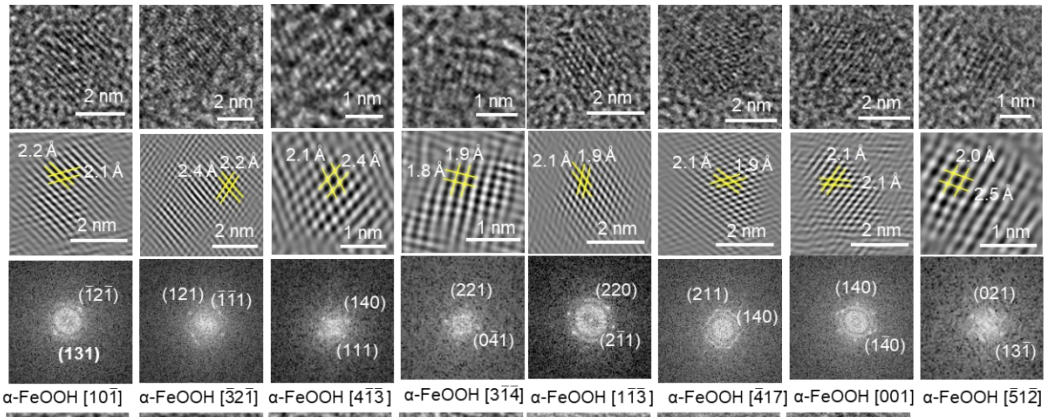
α-FeOOH [10̄1]
α-FeOOH [3̄2̄1]
α-FeOOH [4̄1̄3]
α-FeOOH [3̄1̄4]
α-FeOOH [1̄1̄3]
α-FeOOH [4̄17]
α-FeOOH [001]
α-FeOOH [5̄1̄2]

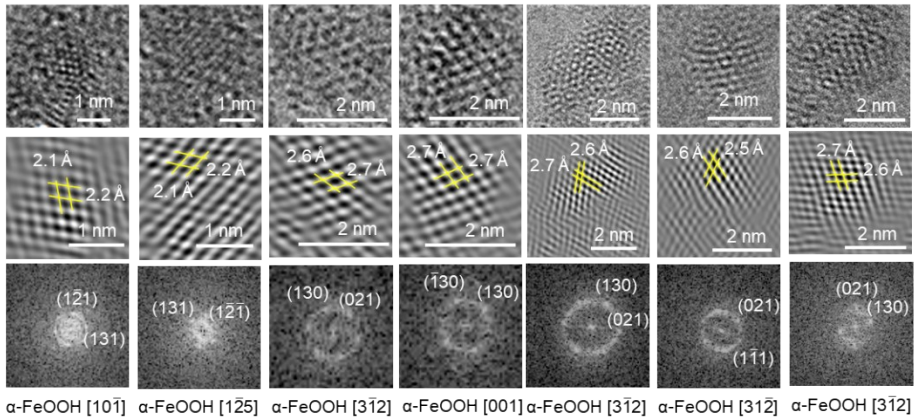
α-FeOOH [10̄1]
α-FeOOH [1̄25]
α-FeOOH [3̄12]
α-FeOOH [001]
α-FeOOH [3̄12]
α-FeOOH [31̄2]
α-FeOOH [3̄12]

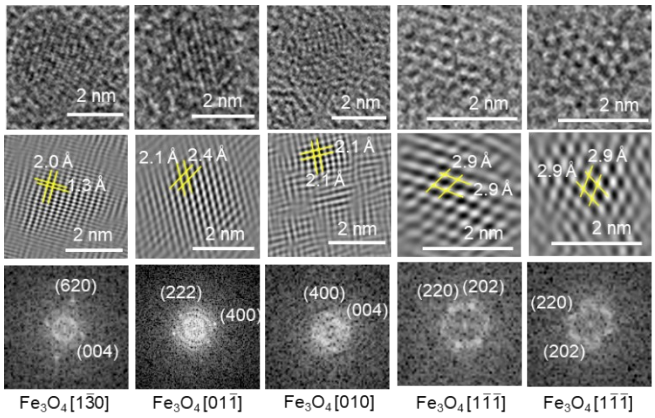

Fig.S5 High resolution SACTEM analysis of the primary IONPs prepared with 0.03 mM reaction concentration at ~ 1 min.

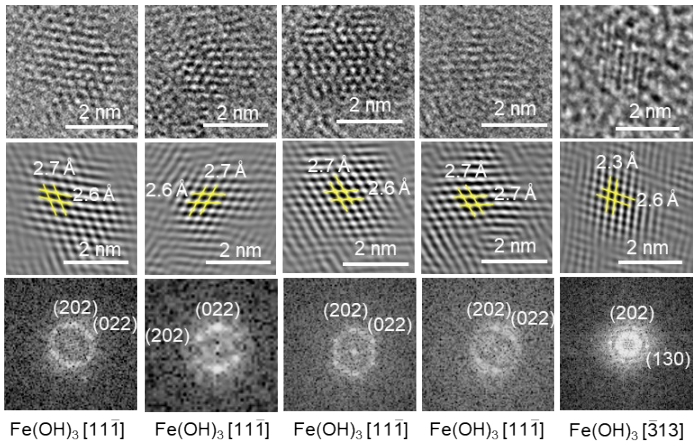

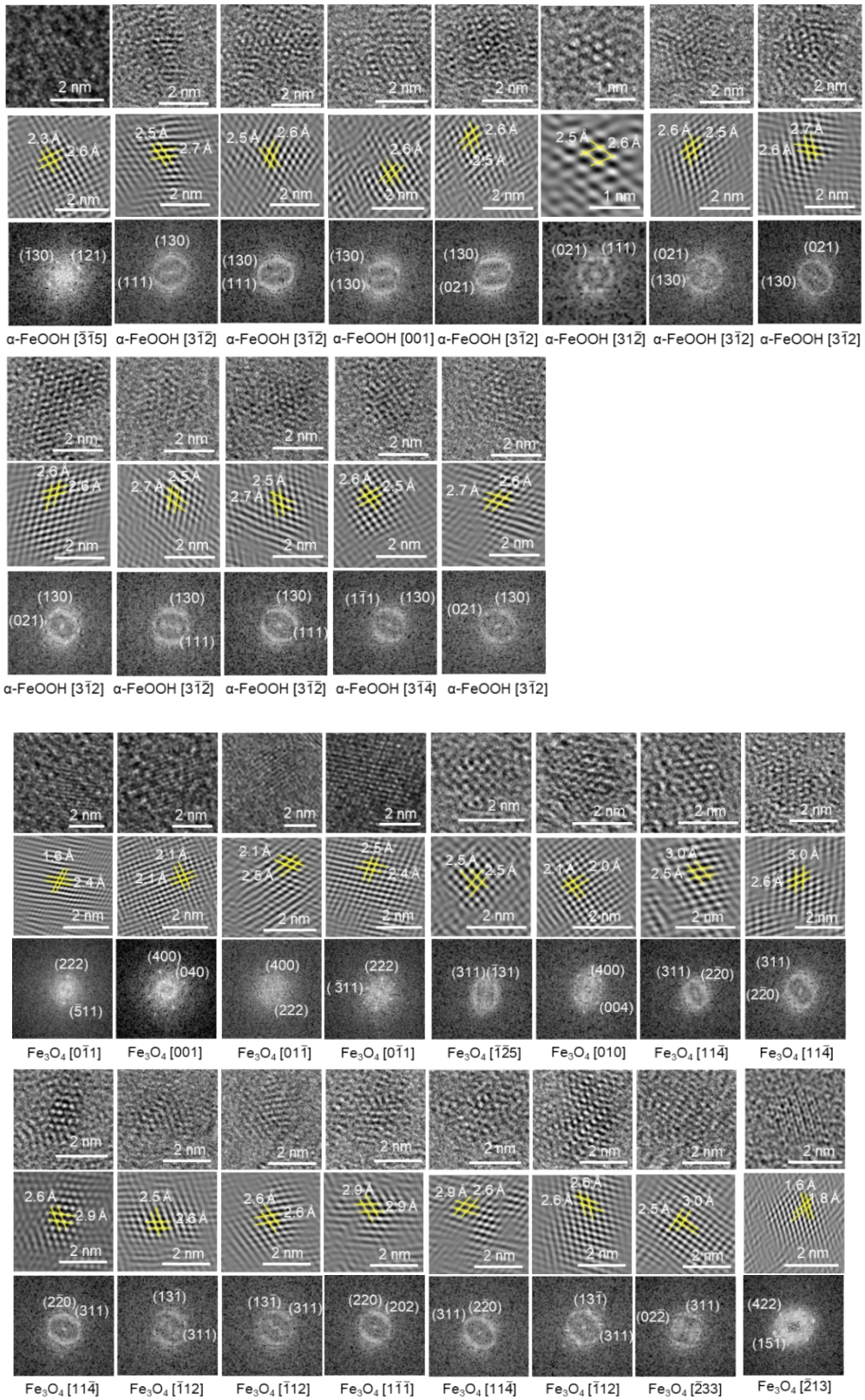

Fig.S6 High resolution SACTEM analysis of the primary IONPs prepared with 0.03 mM reaction concentration at ~ 2 min 30 s.

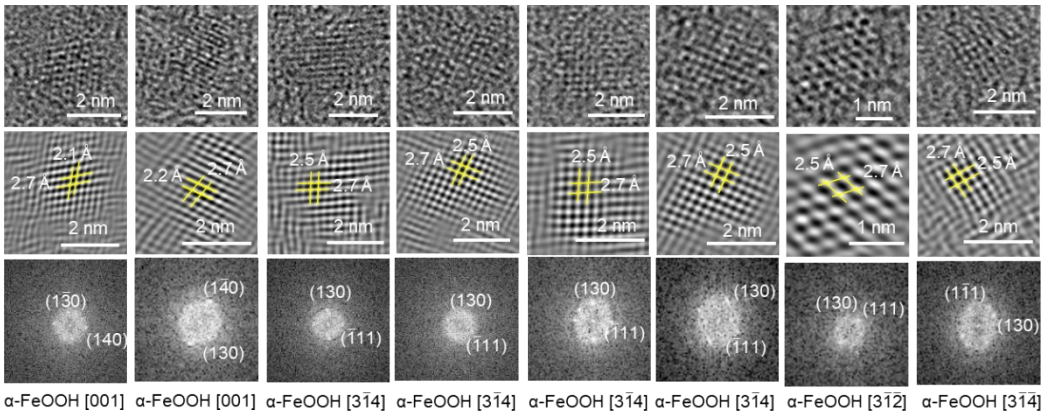
2 nm
1 nm
2.1 Å
2.7 Å
2.2 Å
2.5 Å
(1$\bar{3}$0)
(140)
(1$\bar{4}$0)
(130)
(111)
(1$\bar{1}$1)
α-FeOOH [001]
α-FeOOH [001]
α-FeOOH [3$\bar{1}$4]
α-FeOOH [3$\bar{1}$4]
α-FeOOH [3$\bar{1}$4]
α-FeOOH [3$\bar{1}$4]
α-FeOOH [3$\bar{1}$2]
α-FeOOH [3$\bar{1}$4]

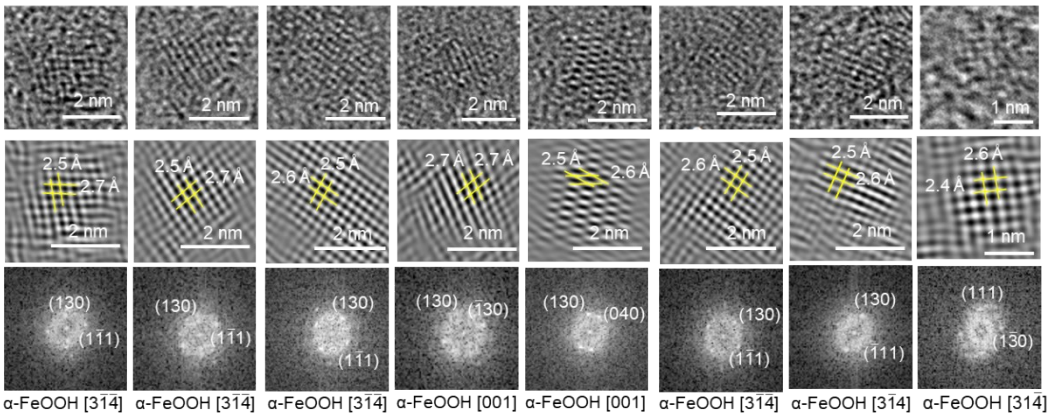
2 nm
1 nm
2.5 Å
2.7 Å
2.6 Å
2.4 Å
(130)
(1$\bar{1}$1)
(040)
(111)
α-FeOOH [3$\bar{1}$4]
α-FeOOH [3$\bar{1}$4]
α-FeOOH [3$\bar{1}$4]
α-FeOOH [001]
α-FeOOH [001]
α-FeOOH [3$\bar{1}$4]
α-FeOOH [3$\bar{1}$4]
α-FeOOH [3$\bar{1}$4]

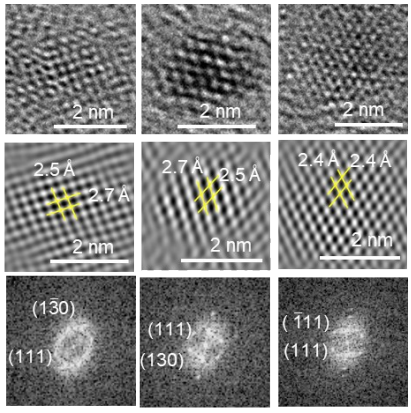
2 nm
2.5 Å
2.7 Å
2.4 Å
(1$\bar{3}$0)
(111)
($\bar{1}$11)
α-FeOOH [3$\bar{1}$4]
α-FeOOH [3$\bar{1}$2]
α-FeOOH [0$\bar{1}$1]

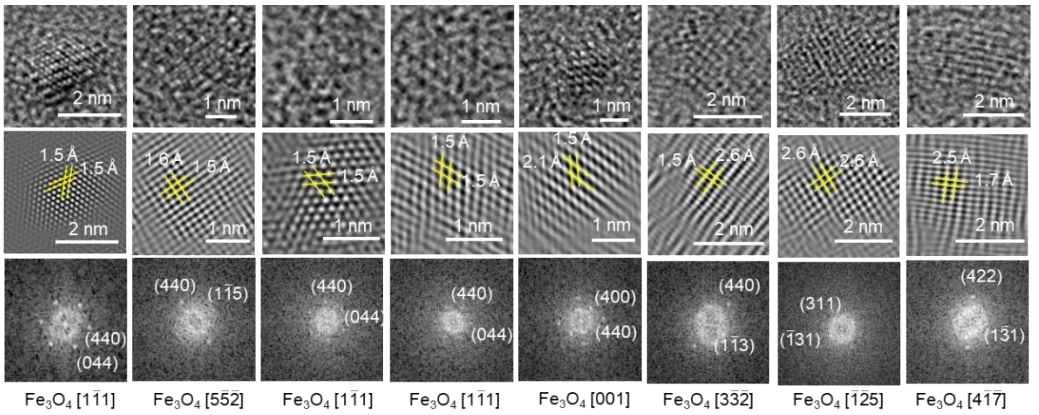
Fe3O4 [1$\bar{1}$1]
Fe3O4 [5$\bar{5}$2]
Fe3O4 [1$\bar{1}$1]
Fe3O4 [1$\bar{1}$1]
Fe3O4 [001]
Fe3O4 [33$\bar{2}$]
Fe3O4 [$\bar{1}$25]
Fe3O4 [4$\bar{1}\bar{7}$]
Fe3O4 [4$\bar{1}\bar{7}$]
Fe3O4 [0$\bar{1}$1]
Fe3O4 [$\bar{2}$55]
Fe3O4 [001]
Fe3O4 [001]
Fe3O4 [$\bar{1}$03]
Fe3O4 [10$\bar{3}$]
Fe3O4 [$\bar{2}$33]

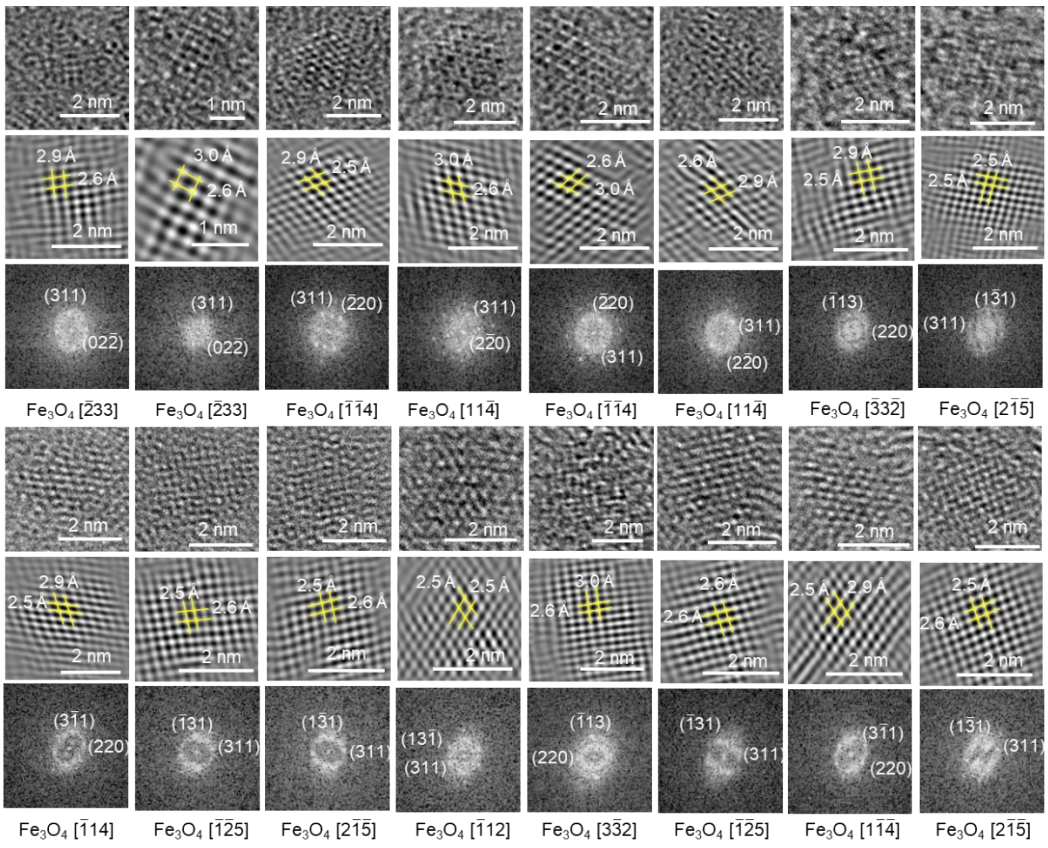
Fe3O4 [$\bar{2}$33]
Fe3O4 [$\bar{2}$33]
Fe3O4 [$\bar{1}\bar{1}$4]
Fe3O4 [11$\bar{4}$]
Fe3O4 [$\bar{1}\bar{1}$4]
Fe3O4 [11$\bar{4}$]
Fe3O4 [3$\bar{3}\bar{2}$]
Fe3O4 [2$\bar{1}\bar{5}$]
Fe3O4 [$\bar{1}$14]
Fe3O4 [$\bar{1}\bar{2}$5]
Fe3O4 [2$\bar{1}\bar{5}$]
Fe3O4 [$\bar{1}$12]
Fe3O4 [3$\bar{3}\bar{2}$]
Fe3O4 [$\bar{1}\bar{2}$5]
Fe3O4 [1$\bar{1}\bar{4}$]
Fe3O4 [2$\bar{1}\bar{5}$]

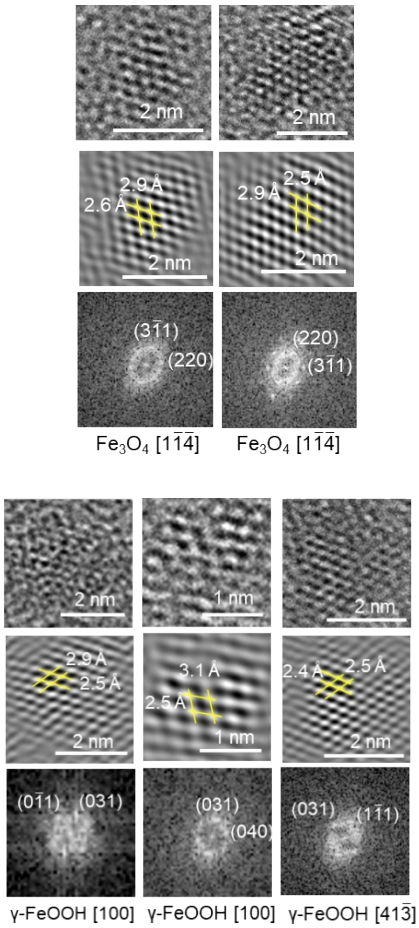

Fig.S7 High resolution SACTEM analysis of the primary IONPs prepared with 0.03 mM reaction concentration at ~ 4 min 12 s.

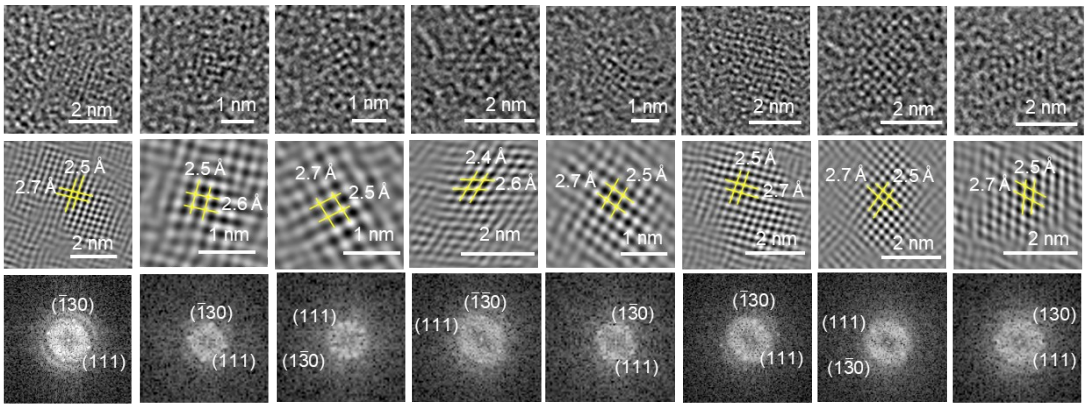

α-FeOOH [31$\bar{4}$] α-FeOOH [31$\bar{4}$] α-FeOOH [31$\bar{4}$] α-FeOOH [3$\bar{1}\bar{2}$] α-FeOOH [31$\bar{4}$] α-FeOOH [31$\bar{4}$] α-FeOOH [31$\bar{4}$] α-FeOOH [3$\bar{1}\bar{2}$]

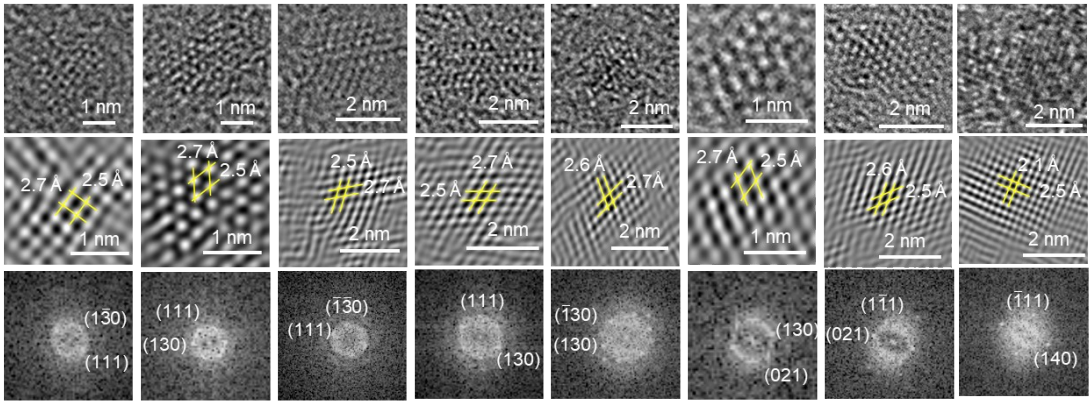

α-FeOOH [31$\bar{4}$] α-FeOOH [3$\bar{1}\bar{2}$] α-FeOOH [3$\bar{1}\bar{2}$] α-FeOOH [3$\bar{1}\bar{2}$] α-FeOOH [001] α-FeOOH [3$\bar{1}\bar{2}$] α-FeOOH [3$\bar{1}\bar{2}$] α-FeOOH [$\bar{4}\bar{1}\bar{5}$]

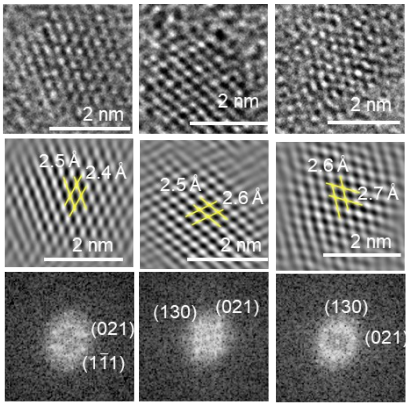

α-FeOOH [3$\bar{1}\bar{2}$] α-FeOOH [3$\bar{1}\bar{2}$] α-FeOOH [3$\bar{1}\bar{2}$]

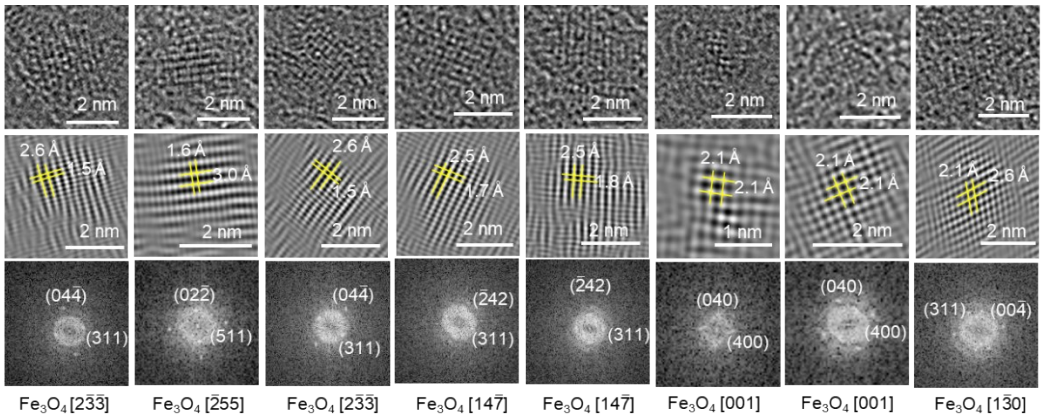

Fe_3O_4 [$2\bar{3}\bar{3}$] Fe_3O_4 [$\bar{2}55$] Fe_3O_4 [$2\bar{3}\bar{3}$] Fe_3O_4 [$14\bar{7}$] Fe_3O_4 [$14\bar{7}$] Fe_3O_4 [001] Fe_3O_4 [001] Fe_3O_4 [$1\bar{3}0$]

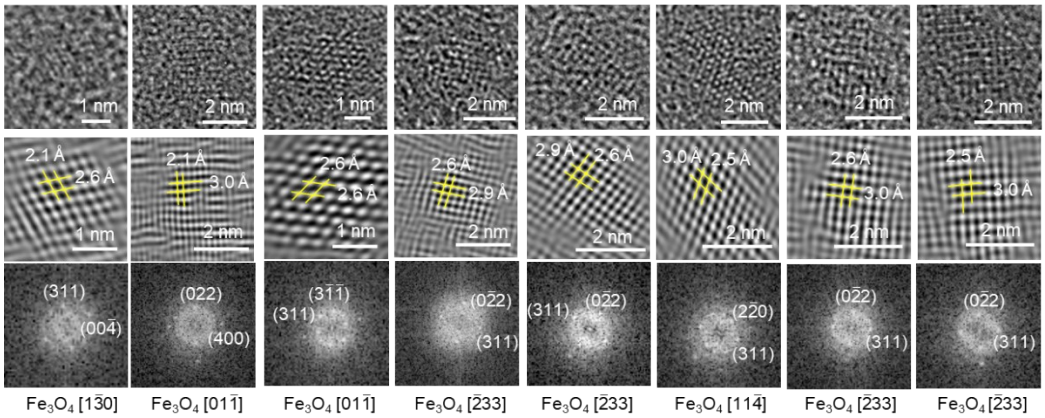

Fe_3O_4 [$1\bar{3}0$] Fe_3O_4 [$01\bar{1}$] Fe_3O_4 [$01\bar{1}$] Fe_3O_4 [$\bar{2}33$] Fe_3O_4 [$\bar{2}33$] Fe_3O_4 [$11\bar{4}$] Fe_3O_4 [$\bar{2}33$] Fe_3O_4 [$\bar{2}33$]

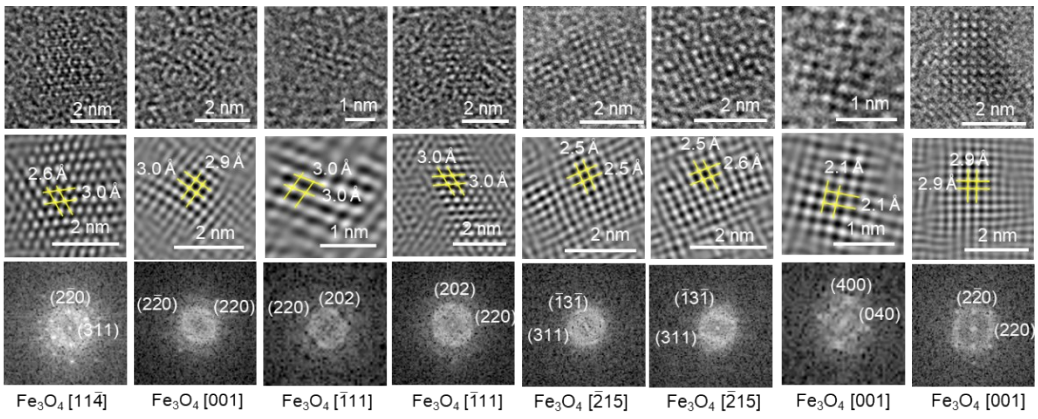

Fe_3O_4 [$11\bar{4}$] Fe_3O_4 [001] Fe_3O_4 [$\bar{1}11$] Fe_3O_4 [$\bar{1}11$] Fe_3O_4 [$\bar{2}15$] Fe_3O_4 [$\bar{2}15$] Fe_3O_4 [001] Fe_3O_4 [001]

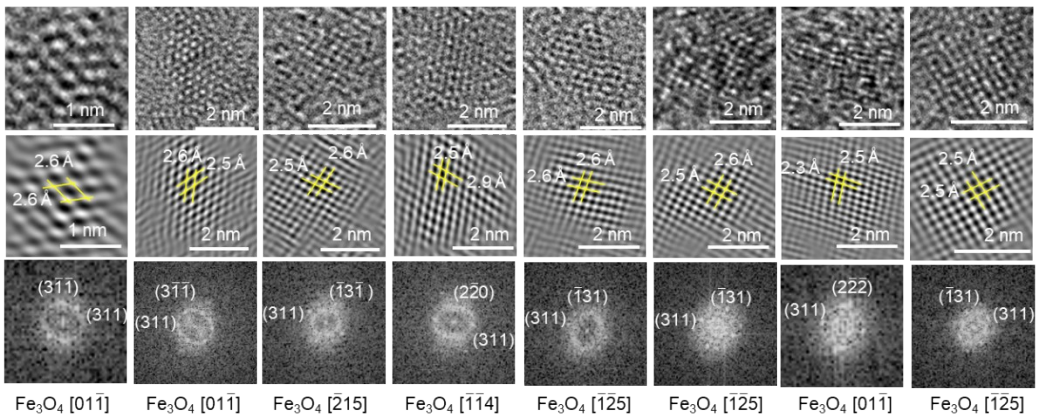

Fe_3O_4 [$01\bar{1}$] Fe_3O_4 [$01\bar{1}$] Fe_3O_4 [$\bar{2}15$] Fe_3O_4 [$\bar{1}\bar{1}4$] Fe_3O_4 [$\bar{1}25$] Fe_3O_4 [$\bar{1}25$] Fe_3O_4 [$01\bar{1}$] Fe_3O_4 [$\bar{1}25$]

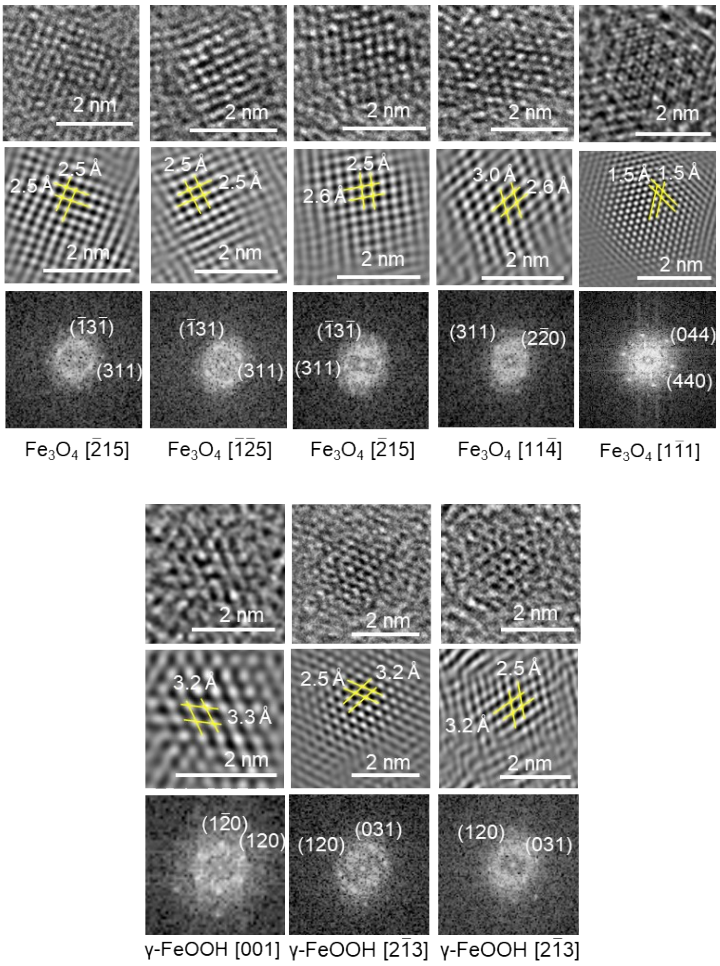

Fig.S8 High resolution SACTEM analysis of the primary IONPs prepared with 0.03 mM reaction concentration at ~ 5 min 40 s.

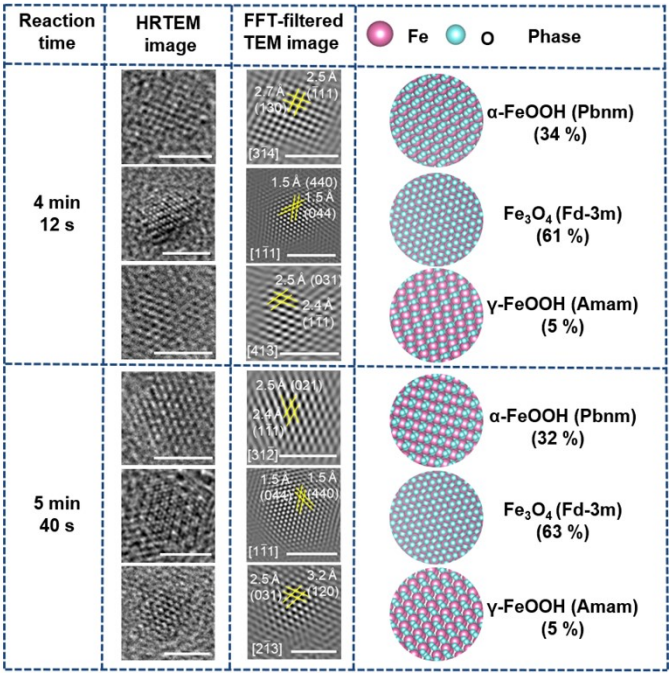

Fig.S9 High resolution ACTEM images, fast fourier transform (FFT) filtered TEM images and the schematic lattice models along the determined crystal zone axes of primary IONPs prepared with 0.03 mM iron precursor concentrations at 4 min 12 s and 5 min 40 s (scale bar: 2 nm).

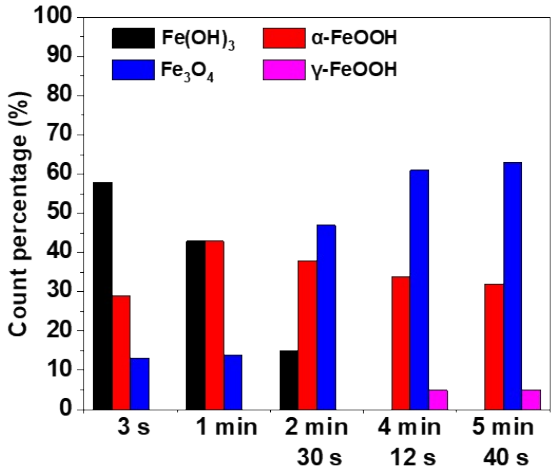

Fig.S10 The percentage of the different phases of the primary IONPs as a function of reaction time.The reactions were performed with 0.03 mM iron precursor concentrations.

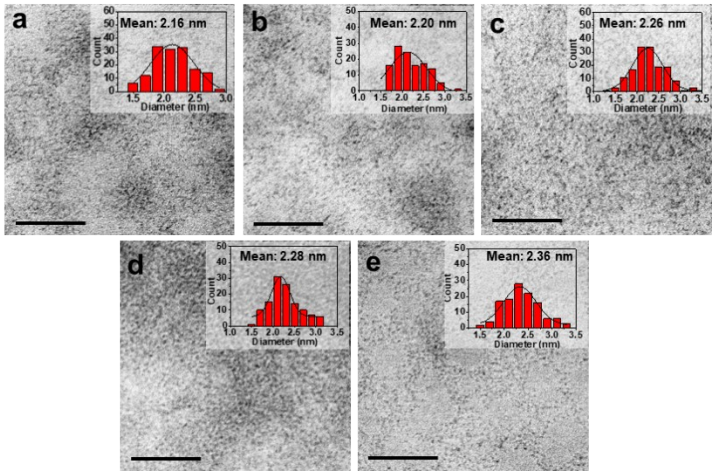

Fig.S11 STEM images under BF mode of the primary IONPs prepared with 0.3 mM iron precursor at (a) 3 s, (b) 1 min, (c) 2 min 30 s, (d) 4 min 12 s and (e) 5 min 40 s (scale bar, 20 nm).

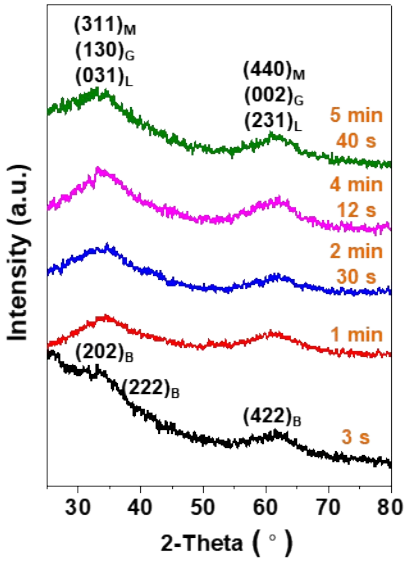

Fig.S12 Synchrotron X-ray diffraction patterns of primary IONPs prepared with 0.3 mM iron precursor at different reaction times (3 s, 1 min, 2 min 30 s, 4 min 12 s and 5 min 40 s). The subscription B, G, L and M represent the $Fe(OH)_3$ (JCPDS no. 46-1436), α-FeOOH (JCPDS no. 29-0713), γ-FeOOH (JCPDS no. 76-2301), and Fe_3O_4 (JCPDS no. 19-0629) phase, respectively.

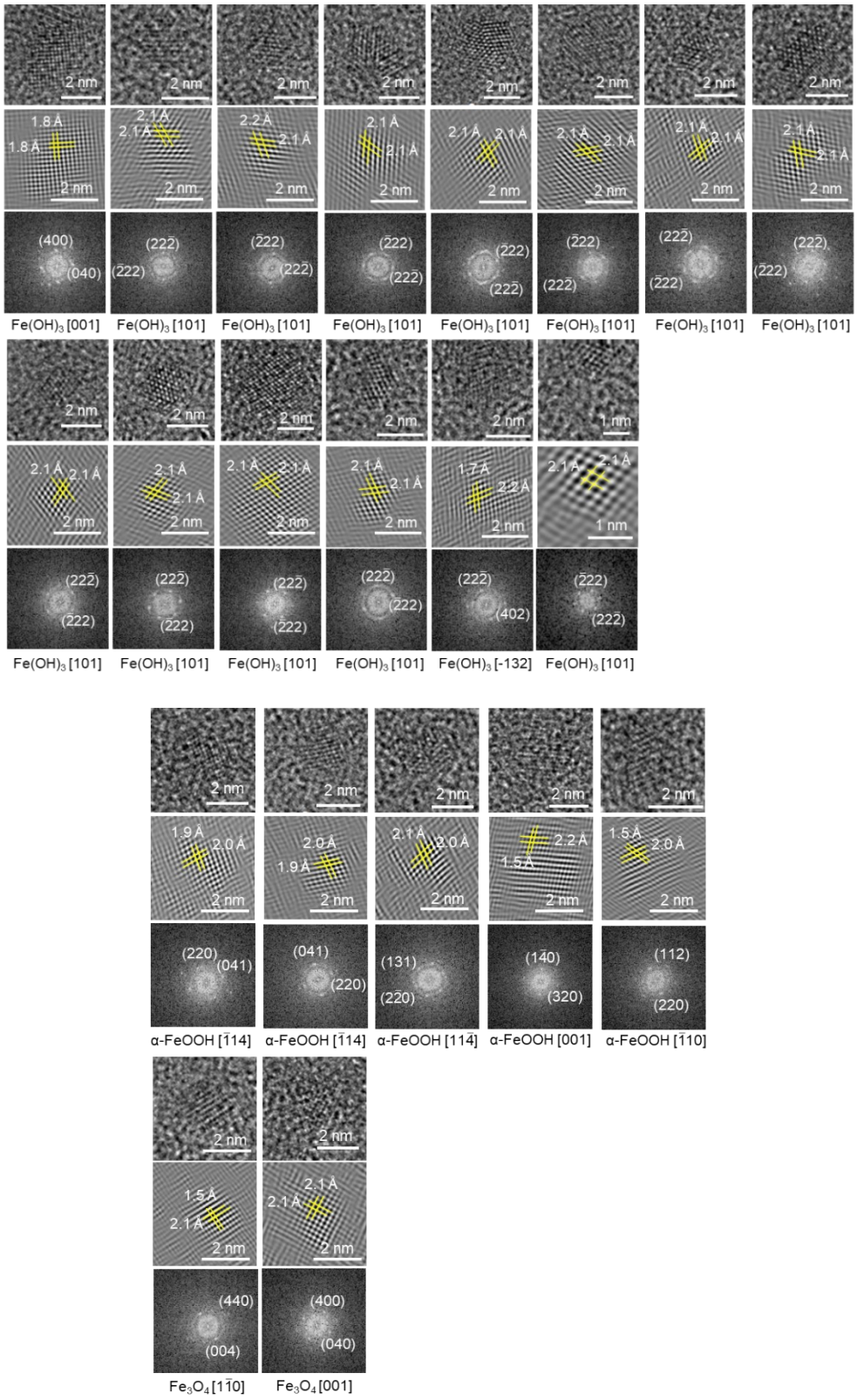

Fig.S13 High resolution SACTEM analysis of the primary IONPs prepared with 0.3 mM reaction concentration at ~ 3 s.

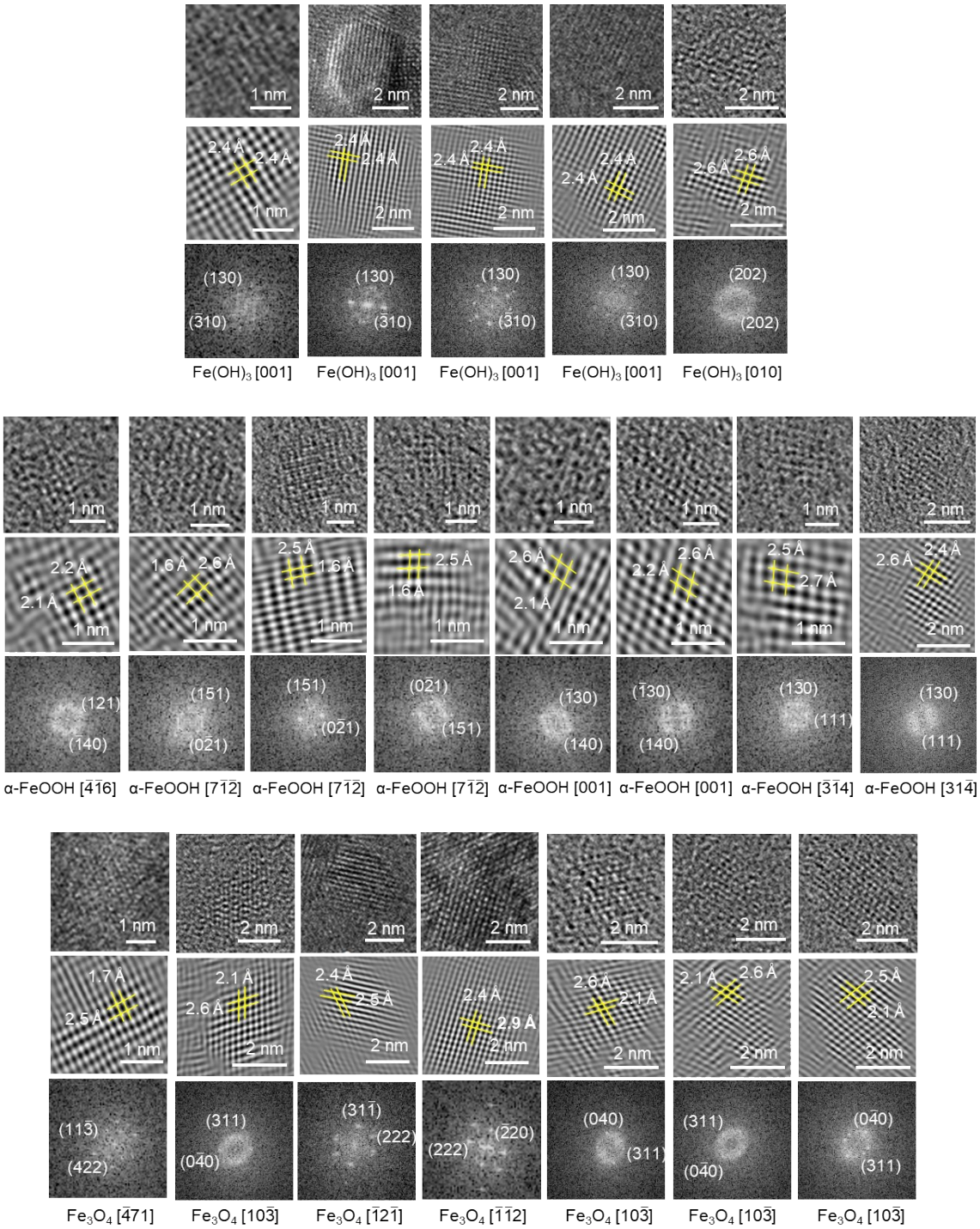

Fig.S14 High resolution SACTEM analysis of the primary IONPs prepared with 0.3 mM reaction concentration at ~ 1 min.

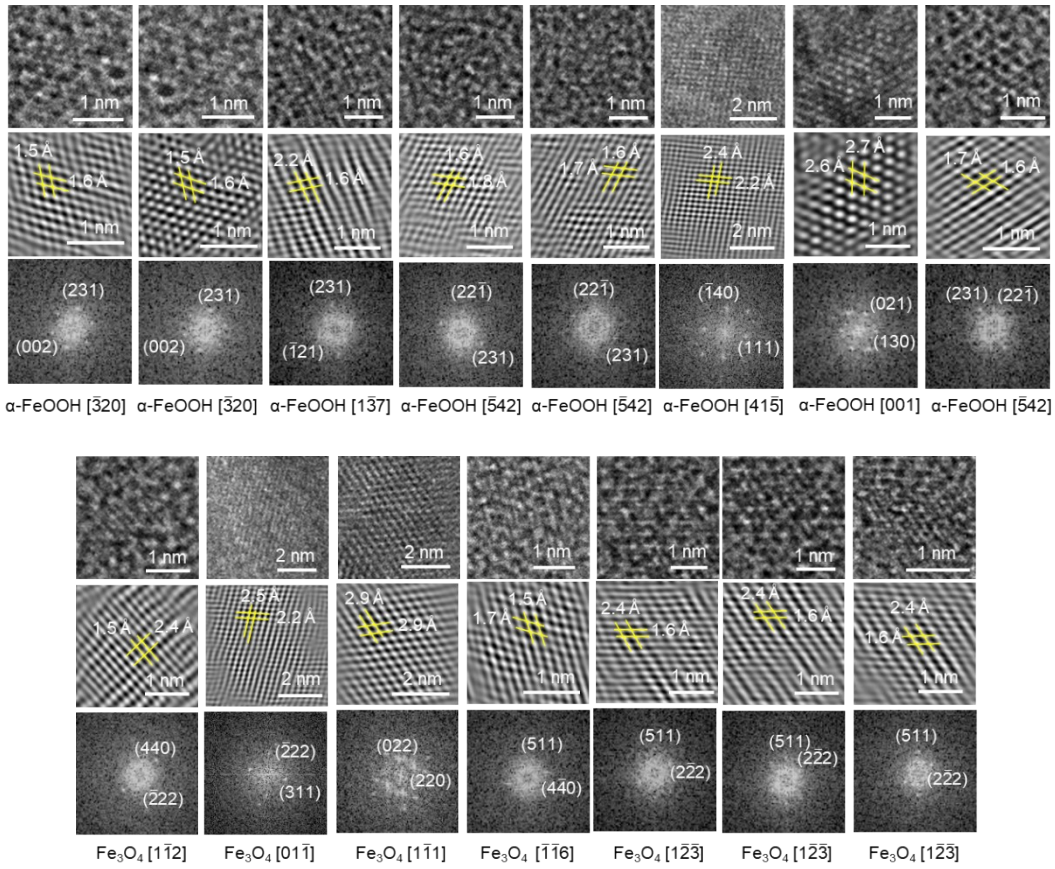

Fig.S15 High resolution SACTEM analysis of the primary IONPs prepared with 0.3 mM reaction concentration at ~ 2 min 30 s.

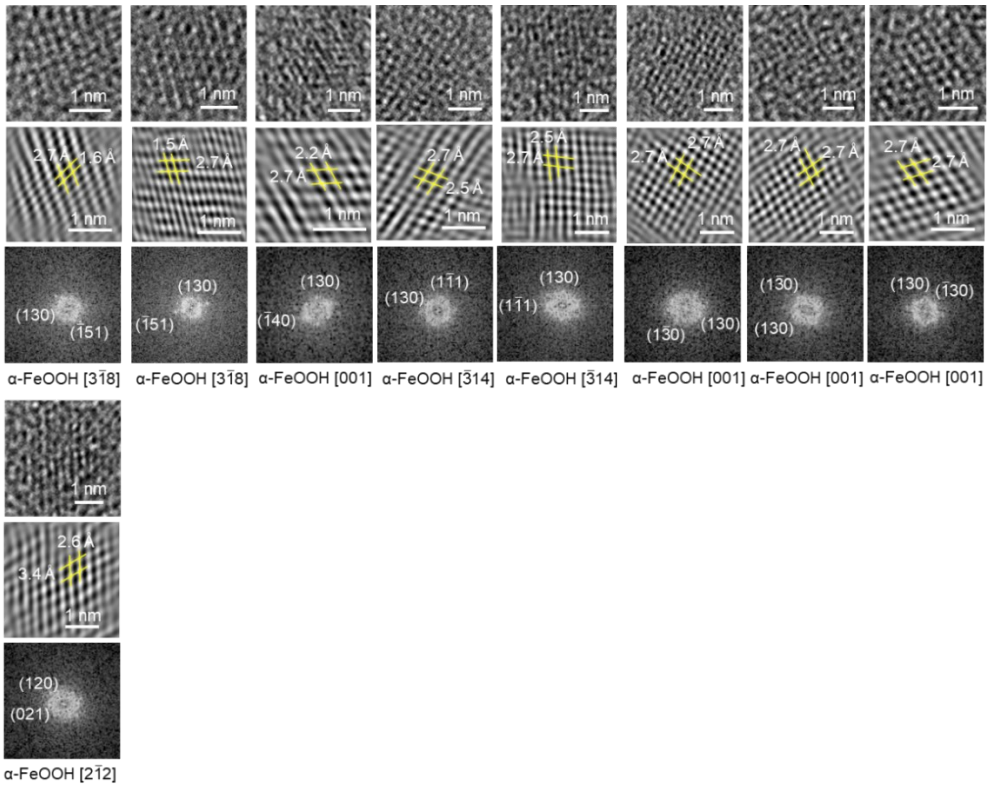

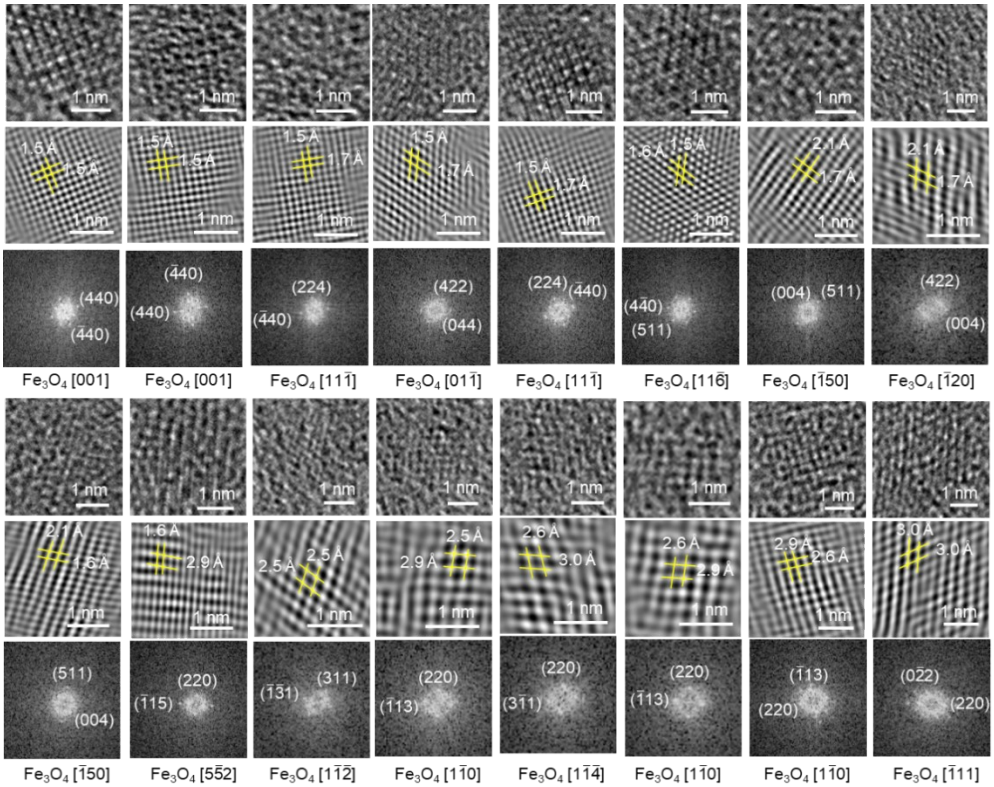

Fig.S16 High resolution SACTEM analysis of the primary IONPs prepared with 0.3 mM reaction concentration at ~ 4 min 12 s.

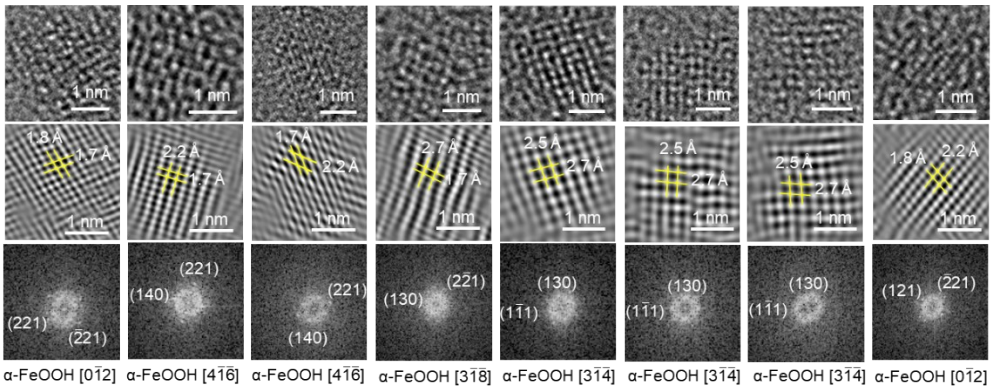

α-FeOOH [0$\bar{1}$2] α-FeOOH [4$\bar{1}$6] α-FeOOH [4$\bar{1}$6] α-FeOOH [3$\bar{1}$8] α-FeOOH [3$\bar{1}$4] α-FeOOH [3$\bar{1}$4] α-FeOOH [3$\bar{1}$4] α-FeOOH [0$\bar{1}$2]

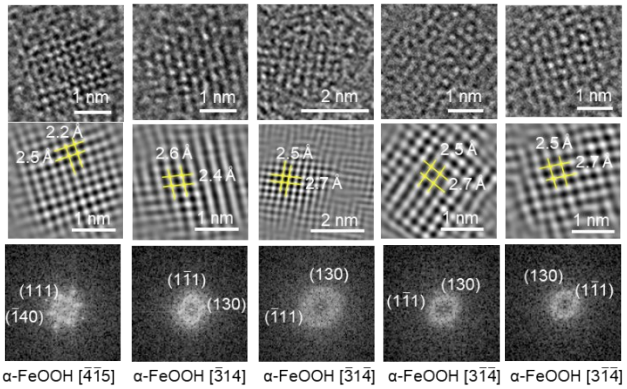

α-FeOOH [4$\bar{1}$5] α-FeOOH [3$\bar{1}$4] α-FeOOH [3$\bar{1}$4] α-FeOOH [3$\bar{1}$4] α-FeOOH [3$\bar{1}$4]

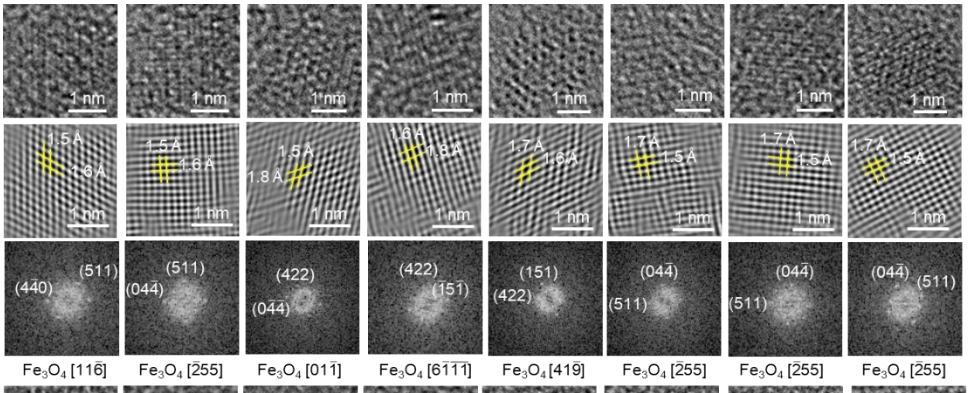

Fe_3O_4 [11$\bar{6}$] Fe_3O_4 [$\bar{2}$55] Fe_3O_4 [01$\bar{1}$] Fe_3O_4 [6$\bar{1}\bar{1}$1] Fe_3O_4 [41$\bar{9}$] Fe_3O_4 [$\bar{2}$55] Fe_3O_4 [$\bar{2}$55] Fe_3O_4 [$\bar{2}$55]

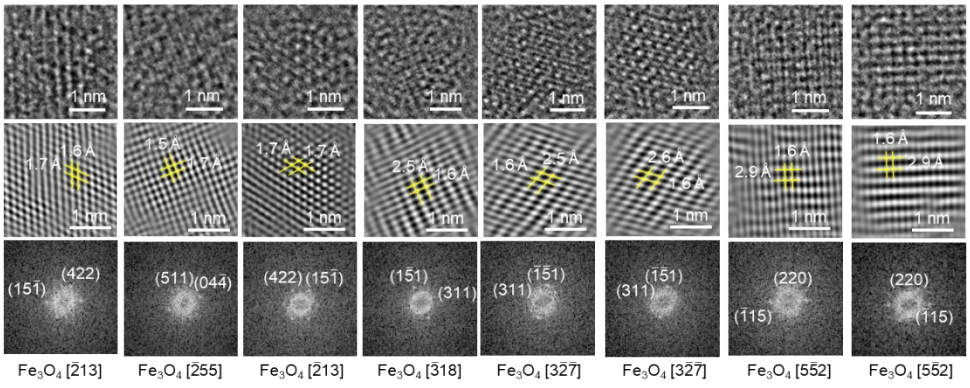

Fe_3O_4 [$\bar{2}$13] Fe_3O_4 [$\bar{2}$55] Fe_3O_4 [$\bar{2}$13] Fe_3O_4 [$\bar{3}$18] Fe_3O_4 [3$\bar{2}\bar{7}$] Fe_3O_4 [3$\bar{2}\bar{7}$] Fe_3O_4 [5$\bar{5}$2] Fe_3O_4 [5$\bar{5}$2]

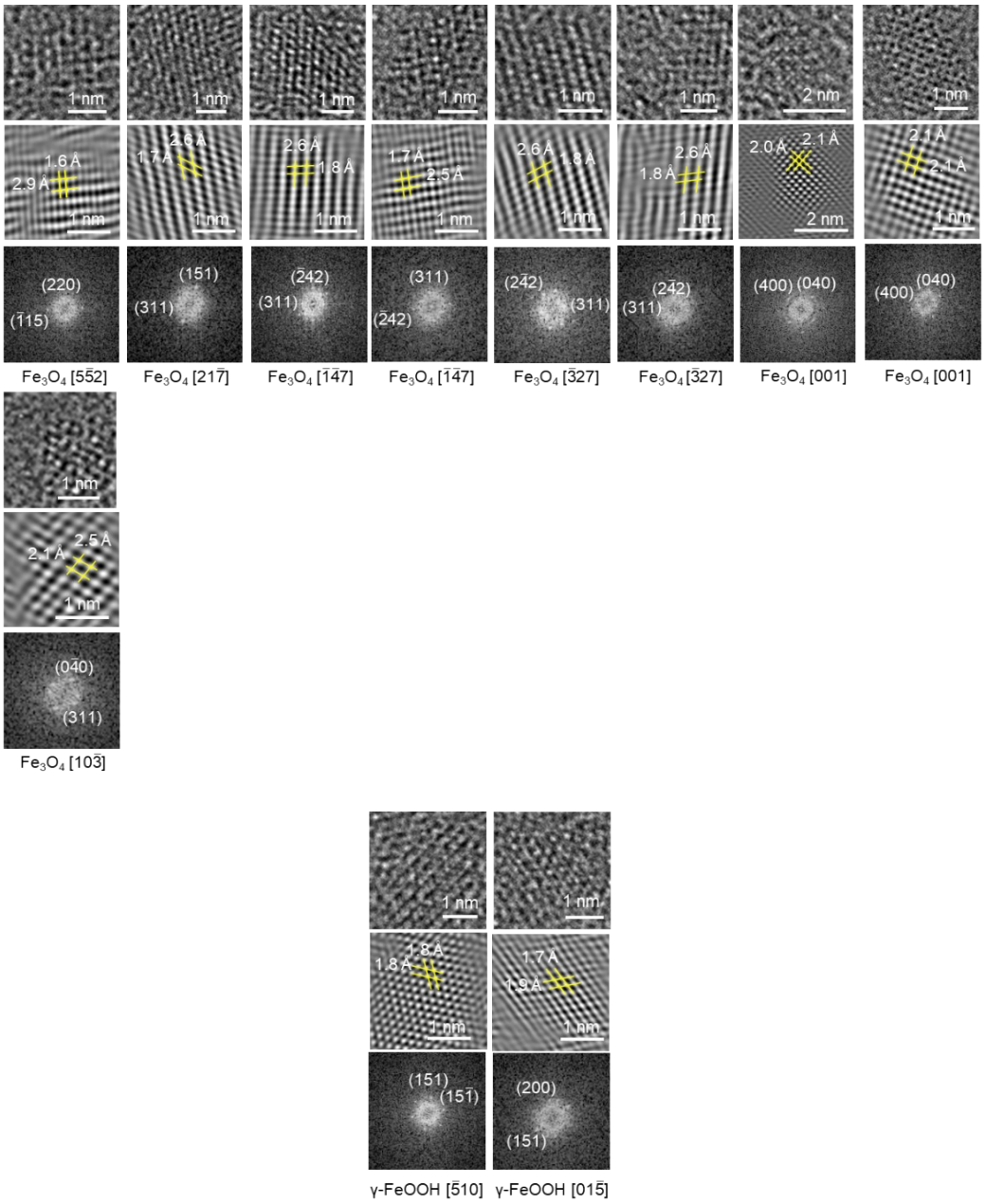

Fig.S17 High resolution SACTEM analysis of the primary IONPs prepared with 0.3 mM reaction concentration at ~ 5 min 40 s.

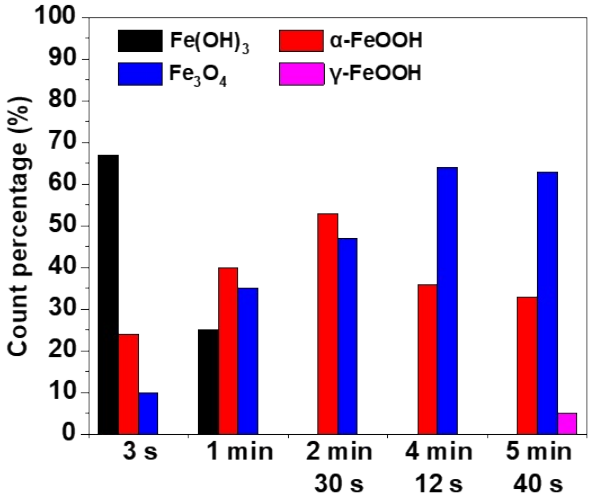

Fig.S18 The percentage of the different phases of the primary IONPs as a function of reaction time. The reactions were performed with 0.3 mM iron precursor concentrations.

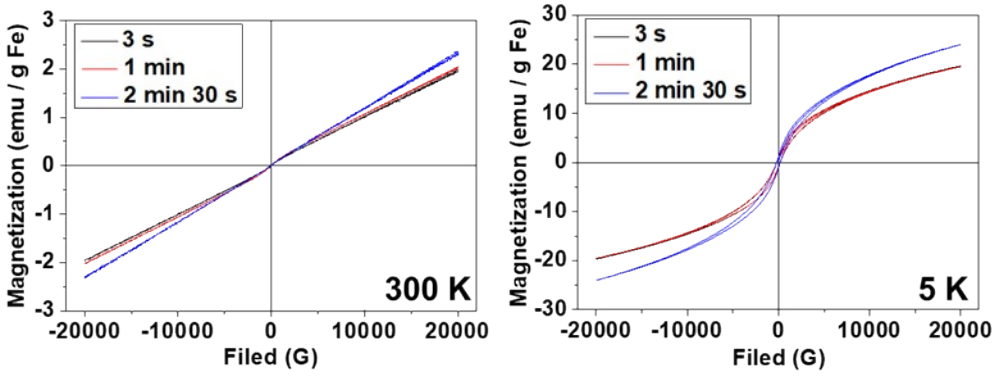

Fig.S19 Field-dependent magnetization curves at 300 K and 5 K of primary IONPs prepared with 0.3 mM precursor solution at different reaction time. The magnetization intensity of the product was enhanced as the reaction time increased. This might be due to the increased content of the magnetic phase Fe_3O_4.

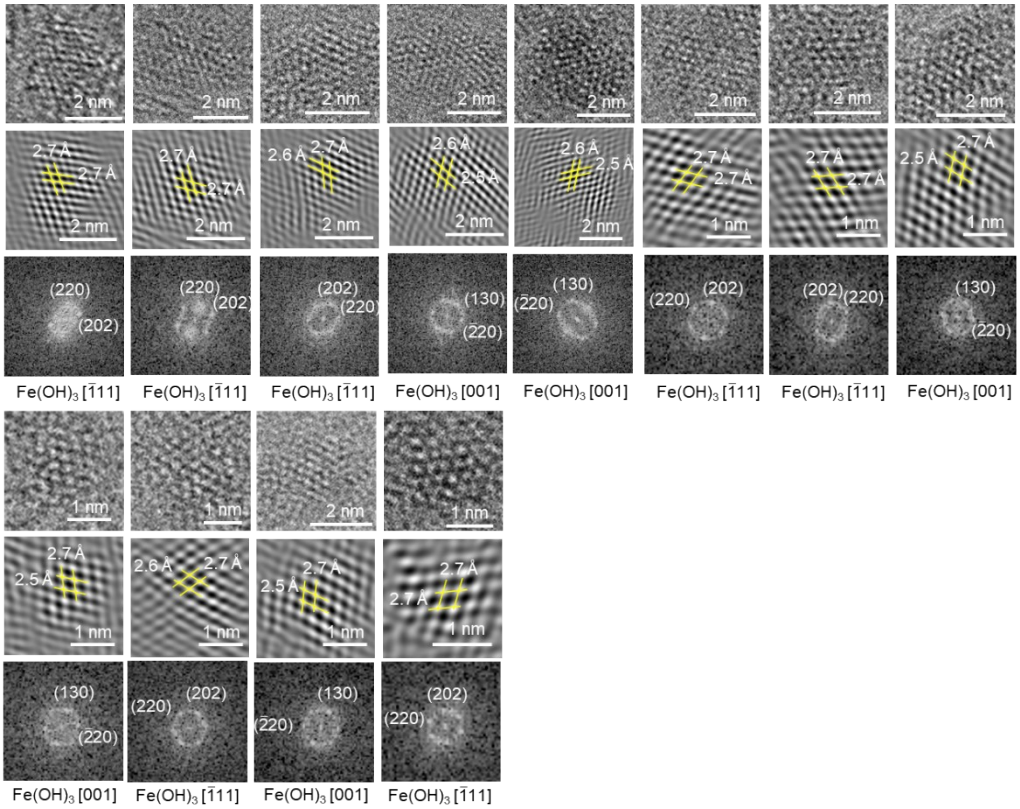

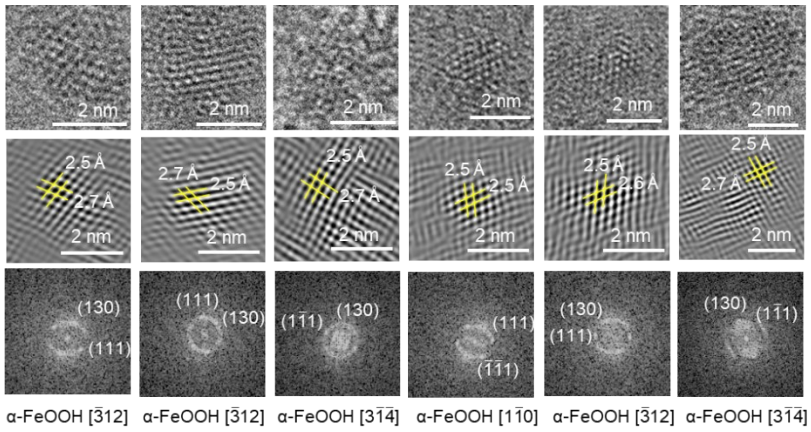

Fig.S20 High resolution TEM analysis of the primary IONPs prepared with 0.02 mM Fe^{3+} at ~ 3 s.

Table S1. The synthesis conditions of primary IONPs samples.

No.	C Fe^{2+} (mM)	C Fe^{3+} (mM)	CPSC (μg/ml)	Final pH	Tube length	Residence time
1	0.01	0.02	7.2	~ 11.2	15 cm	~3 s
2	0.01	0.02	7.2	~ 11.1	4 m	~1 min
3	0.01	0.02	7.2	~ 10.9	10 m	~2 min 30 s
4	0.01	0.02	7.2	~ 10.8	15 m	~4 min 12 s
5	0.01	0.02	7.2	~ 11.0	20 m	~5 min 40 s
6	0.10	0.20	72.0	~ 11.2	15 cm	~3 s
7	0.10	0.20	72.0	~ 11.2	4 m	~1 min
8	0.10	0.20	72.0	~ 11.0	10 m	~2 min 30 s
9	0.10	0.20	72.0	~ 11.0	15 m	~4 min 12 s
10	0.10	0.20	72.0	~ 11.0	20 m	~5 min 40 s

Table S2. The composition of primary IONPs prepared with different reaction conditions.

Reaction condition	$Fe(OH)_3$	α-FeOOH	Fe_3O_4	γ-FeOOH
0.03 mM, 3 s	~ 58 %	~ 29 %	~ 13 %	-
0.03 mM, 1 min	~ 43 %	~ 43 %	~ 14 %	-
0.03 mM, 2 min 30 s	~ 15 %	~ 38 %	~ 47 %	-
0.03 mM, 4 min 12 s	-	~ 34 %	~ 61 %	~ 5 %
0.03 mM, 5 min 40 s	-	~ 33 %	~ 62 %	~ 5%
0.3 mM, 3 s	~ 67 %	~ 24 %	~ 10 %	-
0.3 mM, 1 min	~ 25 %	~ 40 %	~ 35 %	-
0.3 mM, 2 min 30 s	-	~ 53 %	~ 47 %	-
0.3 mM, 4 min 12 s	-	~ 36 %	~ 64 %	-
0.3 mM, 5 min 40 s	-	~ 33 %	~ 63 %	~ 5 %

References

1. M. O. Besenhard, A. P. LaGrow, A. Hodzic, M. Kriechbaum, L. Panariello, G. Bais, K. Loizou, S. Damilos, M. M. Cruz, N. T. K. Thanh and A. Gavriilidis, *Chem Eng J*, 2020, **399**.
2. J. Mahin, C. O. Franck, L. Fanslau, H. K. Patra, M. D. Mantle, L. Fruk and L. Torrente-Murciano, *React Chem Eng*, 2021, **6**, 1961-1973.
3. A. P. LaGrow, M. O. Besenhard, A. Hodzic, A. Sergides, L. K. Bogart, A. Gavriilidis and N. T. K. Thanh, *Nanoscale*, 2019, **11**, 6620-6628.
4. K. Momma and F. Izumi, *J Appl Crystallogr*, 2011, **44**, 1272-1276.
5. W. S. Z. He, S. Jiao, T. Wang, *Principles of chemical engineering*, China Medical Science and Technology Press, Beijing:China, 2015.
6. B. Z. G. Wang, X. Liu, X. Bi, *Inorganic chemistry*, Medical Science and Technology Press, Beijing:China, 2015.